coatings

MDPI

Article

Hydrothermal In-Situ Synthesis and Anti-Corrosion Performance of Zinc Oxide Hydroxyapatite Nanocomposite Anti-Corrosive Pigment

Xiaohong Xu, Huali Wang *, Jianfeng Wu, Zhichao Chen, Xinyi Zhang and Meiqin Li

State Key Laboratory of Silicate Materials for Architectures, Wuhan University of Technology, Wuhan 430070, China; xh@whut.edu.cn (X.X.); jf@whut.edu.cn (J.W.); zhichaochen1@163.com (Z.C.); xinyiz@whut.edu.cn (X.Z.); A15770670769@163.com (M.L.)
* Correspondence: 290684@whut.edu.cn; Tel.: +86-136-6718-3703

Abstract: With the rapid development of the Chinese marine economy, the anti-corrosion of ships and marine engineering facilities has become urgent to be solved. In this paper, a stable zinc-hydroxyapatite (ZnO-HAP) nanocomposite anti-corrosive pigment was prepared by using the hydrothermal in situ synthesis technique, which supported nano-ZnO onto the hydroxyapatite (HAP) surface. The phase composition, microstructure, and performance of the ZnO-HAP nanocomposite were investigated by X-ray diffraction (XRD), Fourier transform infrared (FT-IR), electron probe microanalysis (EPMA), and electrochemical impedance spectroscopy (EIS), and the anti-corrosion mechanism of the ZnO-HAP nanocomposite was discussed. The results show that the corrosion resistance of the ZnO-HAP/epoxy is better than that of the pure epoxy resin coating. The optimum condition to fabricate ZnO-HAP/epoxy with suitable corrosion resistance was found to be a ZnO/HAP ratio of 0.65/0.35. The synergistic complementation mechanism of ZnO and HAP enriches the metallic anti-corrosion theory and provides a new idea for the synthesis of novel and promising anti-corrosive pigments.

Keywords: anti-corrosive pigment; ZnO-HAP nanocomposites; hydrothermal in situ synthesis; electrochemical measurement

Citation: Xu, X.; Wang, H.; Wu, J.; Chen, Z.; Zhang, X.; Li, M. Hydrothermal In-Situ Synthesis and Anti-Corrosion Performance of Zinc Oxide Hydroxyapatite Nanocomposite Anti-Corrosive Pigment. *Coatings* **2022**, *12*, 420. https://doi.org/10.3390/coatings12040420

Academic Editor: Mohamed Gamal Mohamed

Received: 25 February 2022
Accepted: 16 March 2022
Published: 22 March 2022

1. Introduction

Metal corrosion is widely found in daily life and industrial production, causing severe economic loss [1]. It is imperative to explore new anti-corrosive materials to improve the service life of metals. At present, the most widely used method is to coat the organic coating on the surface of metals [2,3]. Epoxy resin is widely used among many organic coatings because of its excellent metal adhesion ability. Nevertheless, epoxy resin is susceptible to aging under long-term ultraviolet radiation, which affects its anti-corrosion performance. In addition, electrolyte diffusion through the pores and defects of the epoxy resin can also lead to corrosion; thus, the barrier performance of the coating is seriously decreased. Therefore, how to improve the anti-corrosion performance of epoxy resin coatings is an urgent problem.

In recent years, researchers have found that nanomaterials' unique physical, chemical, and mechanical performance play an essential role in enhancing the anti-corrosive performance of materials [4]. Zinc oxide (ZnO) is a nanometer particle commonly used in coatings. It is considered to be a multifunctional material because of its unique physical and chemical performance, including non-toxicity, chemical stability, and low cost [5,6]. Compared with other nanoparticles such as TiO_2 and Al_2O_3, ZnO presents a stable surface, easy dispersion, anti-bacterial, aging resistance, and UV shielding [7,8]. ZnO can also fill the pores in the polymer matrix, so it has been widely used in anti-corrosive coatings. However, ZnO has poor compatibility with epoxy resin [9], resulting in easy agglomeration of powder

in epoxy resin. Adding ZnO into epoxy resin will reduce the mechanical performance of the coating and improve the anti-corrosion effect. Therefore, ZnO must be modified to make up for this defect. Hydroxyapatite ($(Ca_{10}(PO_4)_6(OH)_2$), HAP) is an environmentally friendly, non-toxic functional material [10,11], with stable chemical performance [12], good metal adhesion [13], significant adsorption capacity, and low water solubility [14]. The compatibility of the anti-corrosive pigment and epoxy resin can be improved by combining HAP and ZnO. In addition, Xue et al. [15] proved that the rich hydroxyl in hydroxyapatite could replace free Cl^- in the coating to form more stable chlorine apatite and reduce metal damage.

The composite of ZnO and HAP improves the compatibility of the anti-corrosive pigment and metal, reducing the coating porosity and solidifying Cl^-. In this paper, nano-ZnO powders were synthesized on the surface of HAP sheets by the hydrothermal in situ synthesis technique. In other words, after adding zinc acetate dihydrate, Zn^{2+} first interacted with the active groups and the surface of HAP to form zinc hydroxide in situ, which was thermally decomposed into ZnO under alkaline conditions, then formed the ZnO-HAP nanocomposite. The anti-corrosive pigment was added to the epoxy resin to prepare the ZnO-HAP/epoxy composite coating. The anti-corrosive pigments and coatings were characterized by XRD, FT-IR, XPS, and SEM. The anti-corrosive performance of ZnO-HAP nanocomposites on mild steels was studied by the electrochemical method.

2. Materials and Methods

2.1. Materials

ZnO and ZnO-HAP were synthesized from disodium hydrogen phosphate dodecahydrate ($Na_2HPO_4{\cdot}12H_2O$), calcium chloride ($CaCl_2$), zinc acetate dihydrate ($(CH_3COO)_2Zn{\cdot}2H_2O$), sodium hydroxide (NaOH), urea ($CO(NH_2)_2$), and anhydrous ethanol (C_2H_5OH) by Sinopharm Chemical Reagent Co., LTD. (Shanghai, China). Epoxy resin E51 and polyamide 650 curing agent were provided by Shanghai Aotun Chemical Technology Co., LTD. (Shanghai, China). Q235 mild steels were purchased from Dongguan Weida Instrument Co., LTD. (Dongguan, China). Mild steel panels of 40 × 25 × 5 mm acted as metal substrates polished by emery papers of 180–600 mesh.

2.2. Fabrication of HAP Pigment

First, 4.29 g of $Na_2HPO_4{\cdot}12H_2O$ was prepared and dissolved in 50 mL of deionized water, and 2.22 g of $CaCl_2$ was dissolved in 20 mL of deionized water. Then, the solution of $CaCl_2$ was slowly dropped into a solution of Na_2HPO_4, and 3 g of urea as a pH regulator was dissolved into the above solution. The mixture was continuously stirred for 30 min and then poured into hydrothermal reaction kettles. The reactions occurred at 180 °C for 9 h (Equation (1)). After the reactions, the synthetic sample was washed. HAP was obtained after washing and drying at 80 °C for 12 h.

$$6HPO_4{}^{2-} + 10Ca^{2+} + 8OH^- \rightarrow Ca_{10}(PO_4)_6(OH)_2 \downarrow + 6H_2O \quad (1)$$

2.3. Fabrication of ZnO-HAP Nanocomposites Pigment

HAP and $(CH_3COO)_2Zn{\cdot}2H_2O$ were weighed according to the mass ratio of ZnO:HAP (80:20 wt.%, 65:35 wt.%, and 50:50 wt.%). The weighed starting materials were fully dissolved in deionized water to obtain the mixed solutions, then NaOH was added to the mixed solutions to adjust the pH to 14. The mixtures were transferred to Teflon reactors and reacted at the heating temperature of 180 °C for 6 h in an oven (Equations (2) and (3)). In the end, the ZnO-HAP precipitates were washed with deionized water and dried at 80 °C for 12 h in the oven.

$$(CH_3COO)_2Zn + 2OH^- \rightarrow Zn(OH)_2 \downarrow + 2CH_3COO^- \quad (2)$$

$$Zn(OH)_2 \rightarrow ZnO + H_2O \quad (3)$$

2.4. Preparation of Anti-Corrosive Coatings

First, ZnO, HAP, and ZnO-HAP (80:20 wt.%, 65:35 wt.%, 50:50 wt.%) pigments were respectively added to 10 g of epoxy resin (51 wt.%), and the pigments in the epoxy resin were whisked for 30 min to ensure an even spread. Then, 8 g of polyurethane (PU) was added to the above mixtures and stirred for 30 min. After achieving homogenous deconcentration, the commixtures were brushed onto the mild steel panels burnished by emery papers and cleaned by absolute ethyl alcohol beforehand. A TC100 coating thickness gauge was used to measure the thickness of the coatings and control them to 50 ± 5 μm (instrument error: ±(3% + 2 μm)). This thickness was experimentally determined as the most optimal for obtaining the maximum protective properties of the coatings. Finally, the coated mild steel panels were placed in a drying oven at 60 °C and cured for one week. The preparation process of the coating is shown in Figure 1.

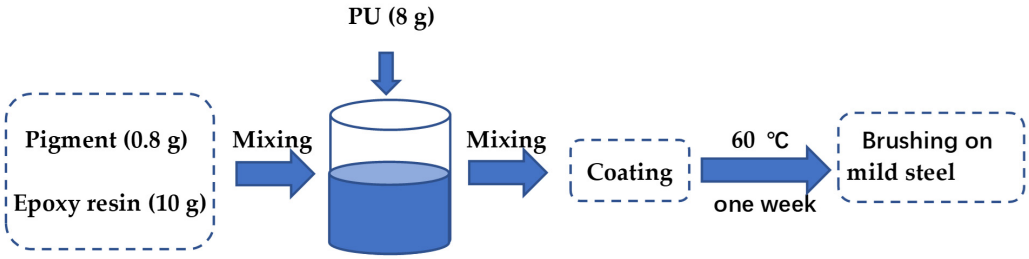

Figure 1. Schematic diagram of the preparation process of the anti-corrosive coating.

2.5. Characterizations

The coating thickness gauge (TC100, Shenzhen Red Dragon Instrument, Shanghai, China) was used to measure the coating thickness. The crystal structures and chemical composition were investigated by X-ray diffractometer (XRD) (Model D/max-IIIA, Rigaku, JEOL, Tokyo, Japan) and infrared spectroscopy (FT-IR) (Nicolet6700, TMO, Waltham, MA, USA). A scanning electron microscope (SEM) (JSM-IT300, JEOL, Tokyo, Japan) was used to analyze the anti-corrosive pigments' morphology and the coatings' section morphology. The dispersibility of the prepared anti-corrosive pigments in the coating was studied by electron probe microanalysis (EPMA) (JSM-IT300, JEOL, Tokyo, Japan) using an optical drop shape analyzer (DropMeter-A-100, Haishu Maishi Scientific Test Co. Ningbo, China). The corrosion resistance of the coatings was tested by an electrochemical workstation (CHI660E, SCE, Shanghai, China). A three-electrode system was used in the electrochemical tests. The mild steel panels served as working electrodes, the saturated calomel electrode as the reference electrode, and the platinum sheet (20 mm × 20 mm × 0.1 mm) as the counter electrode. Polarization curve tests were employed in the frequency range of 10^{-2}~10^{5} Hz with amplitude perturbation of 20 mV. The polarization curves were tested with a scanning rate of 1 mV/s.

3. Results and Discussion

3.1. Characterization of Pigments

To understand the crystal phase composition of anti-corrosive pigments, XRD was used. Figure 2a shows the XRD pattern of HAP. The pattern of HAP was consistent with the standard peaks (PDF card No. 74-0565). The XRD pattern of ZnO is shown in Figure 2b, which was also consistent with the standard peaks (PDF card No. 79-2205). The crystal structures of HAP and ZnO are hexagonal [11,16]. As shown in Figure 2c–e, the peaks of ZnO and HAP were found in the XRD diffraction pattern, and the peaks were consistent with those of spectral ZnO and HAP, which indicates that the synthesized powders are ZnO-HAP nanocomposites.

To explore the influence of the addition of ZnO-HAP nanocomposites on the epoxy resin coating, ZnO-HAP nanocomposites with a ratio of 65 wt.% ZnO and 35 wt.% HAP (a), epoxy resin coating (b), and ZnO-HAP/epoxy resin coating (c) were tested, respectively. The test results are shown in Figure 3. Figure 3a shows the characteristic absorption peaks of the Zn–O bond at 467 and 415 cm^{-1}, the peaks at 1089 and 1031 cm^{-1} are due to the asymmetric stretching of the P-O bond of phosphate groups, the sharp peaks at 604 and 563 cm^{-1} are attributed to the bending modes of the O–P–O bonds in phosphate groups, and the stretching vibration of –OH caused the peaks at 3434 and 604 cm^{-1}. The FT-IR spectra of ZnO-HAP nanocomposites further show that the anti-corrosive pigment is composed of ZnO and HAP, consistent with the XRD results. In Figure 3b, the stretching vibration absorption peaks of the N–H group and –OH were at 3380 cm^{-1} [17]. In Figure 3c, the polymer peaks of ZnO-HAP/epoxy resin show that the characteristic peaks of ZnO and HAP increased, compared with the peaks of pure epoxy resin. In contrast, the position of the peaks remained unchanged, indicating that ZnO-HAP nanocomposites can still exist stably after being added into epoxy resin.

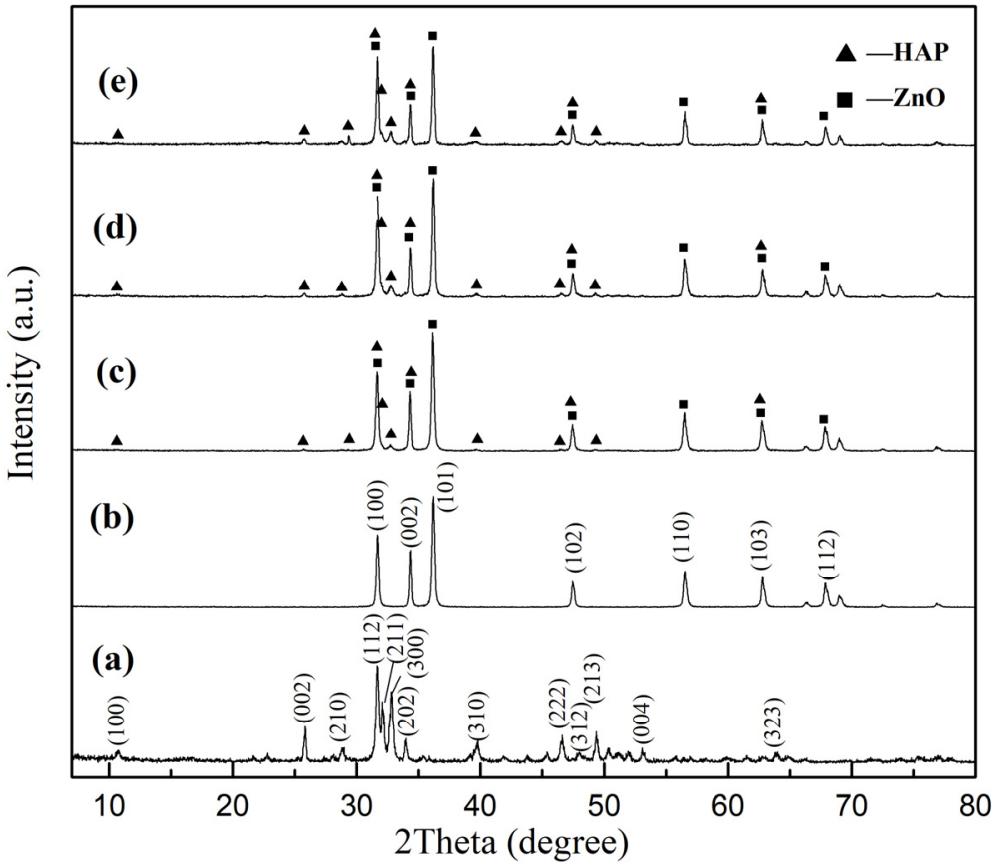

Figure 2. XRD patterns of samples (**a**) HAP, (**b**) ZnO, (**c**) ZnO-HAP (80 wt.% ZnO + 20 wt.% HAP), (**d**) ZnO-HAP (65 wt.% ZnO + 35 wt.% HAP), and (**e**) ZnO-HAP (50 wt.% ZnO + 50 wt.% HAP).

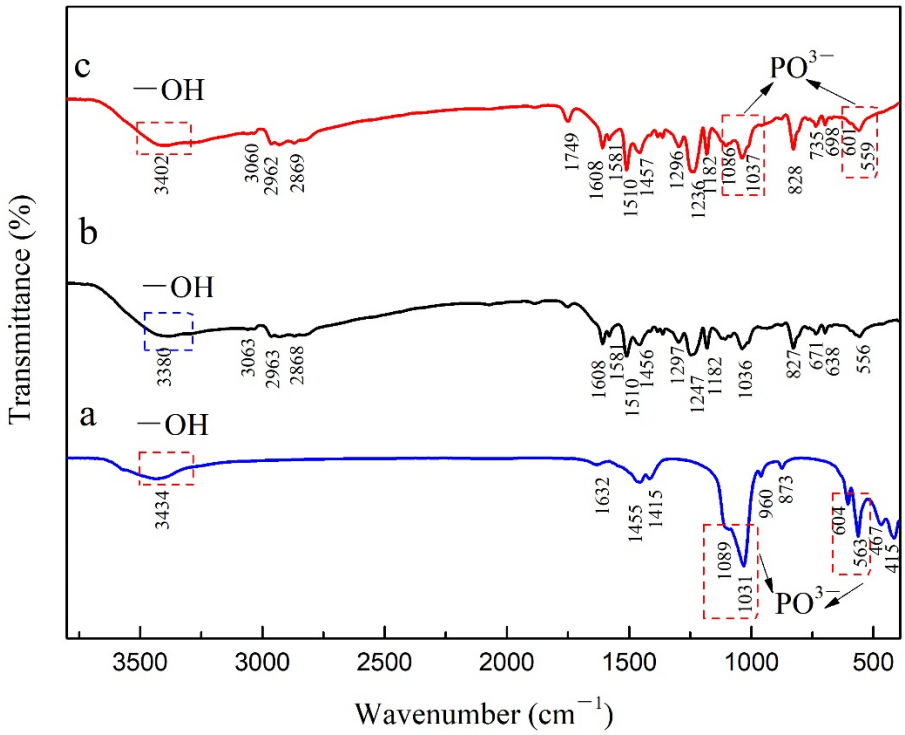

Figure 3. FT-IR spectra of samples (**a**) ZnO-HAP (65 wt.% ZnO + 35 wt.% HAP), (**b**) epoxy resin coating, and (**c**) ZnO-HAP (65 wt.% ZnO + 35 wt.% HAP)/epoxy resin coating.

3.2. Microstructural Analysis

Figure 4a shows ZnO prepared under pH and hydrothermal conditions. The diameter of the ZnO crystal is about 150–200 nm. In Figure 4b, the morphology of ZnO attached to HAP remained unchanged after HAP modification. The element distribution is shown in Figure 5, and the surface elemental composition of ZnO-HAP nanocomposites is analyzed. The EDS patterns of the area scan and three selected spots are exhibited in Figure 6, and the EDS semi-quantitative results are listed in Table 1. The presence of Ca, P, Zn, and O in the images and the distribution of each element proved that ZnO and HAP were successfully combined. ZnO distributed uniformly on the HAP surface, which significantly reduced the accumulation of ZnO nanoparticles. The EDS semi-quantitative results proved that the tiny grains attached to HAP are ZnO.

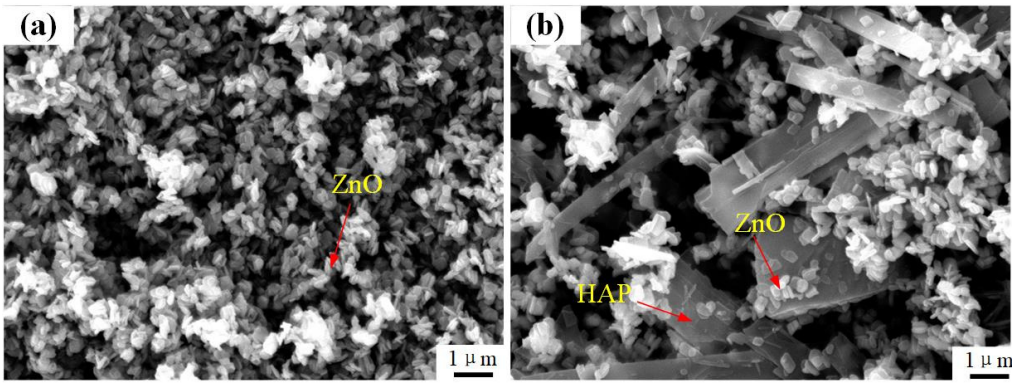

Figure 4. SEM images of (**a**) ZnO and (**b**) ZnO-HAP (65 wt.% ZnO + 35 wt.% HAP).

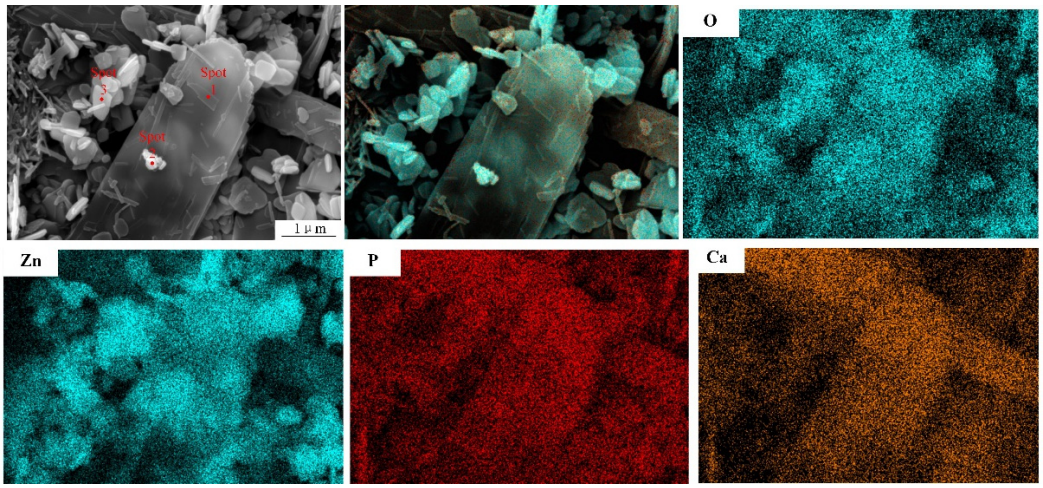

Figure 5. Secondary electron image and element distribution of ZnO-HAP (65 wt.% ZnO + 35 wt.% HAP) powders.

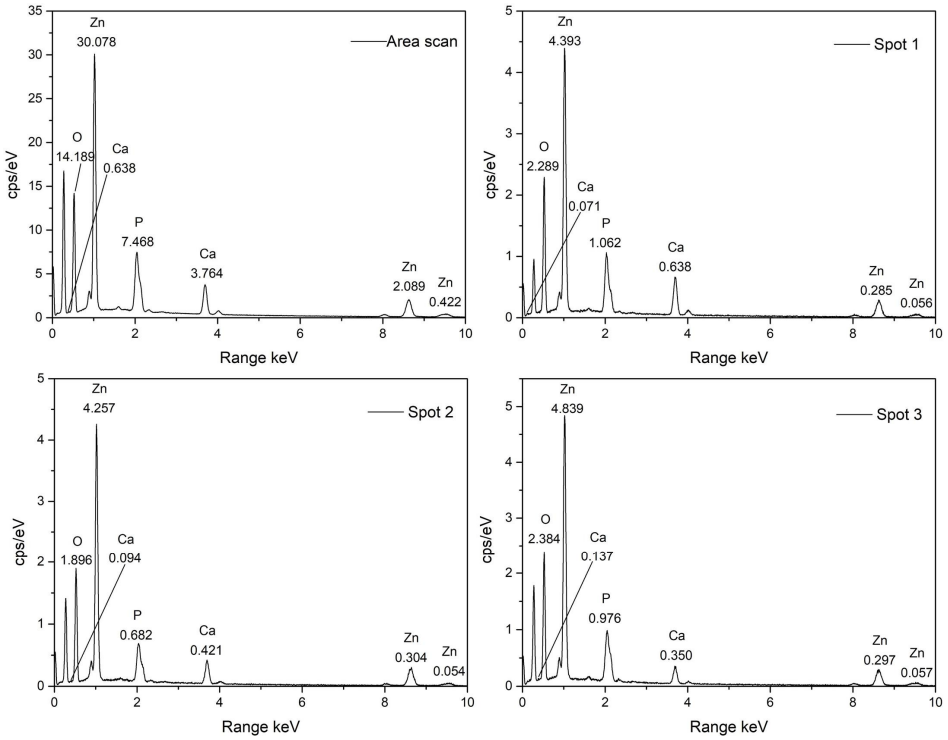

Figure 6. EDS analysis of area scan and three selected spots in Figure 5.

Table 1. EDS analysis results of the area scan and three selected spots shown in Figure 6.

Area (wt.%)	O	Zn	P	Ca	Composition
Total area	29.45	56.54	5.65	8.36	ZnO and HAP
1	30.34	53.80	6.30	9.56	
2	28.75	59.77	4.63	6.85	
3	29.64	61.50	3.94	4.92	

To study the internal structure of the coating, SEM was used to observe the cross-section of the epoxy resin coating after adding the anti-corrosive pigment. Figure 7a shows the fracture surface of the pure epoxy coating, while Figure 7b shows the cross-section of HAP/epoxy resin. From the cross-section of the coating, HAP appears to agglomerate in

the epoxy resin, which will affect the anti-corrosion effect. Figure 7c shows the cross-section of zinc oxide/epoxy resin. No significant accumulation of zinc oxide particles was found. Figure 7d shows the cross-section of ZnO-HAP/epoxy resin with 65% ZnO content. As zinc oxide was attached to the HAP surface, HAP agglomeration improved. ZnO-HAP was evenly distributed in the epoxy resin coating, which increases the density of the coating and makes the diffusion channel of the electrolyte more complicated.

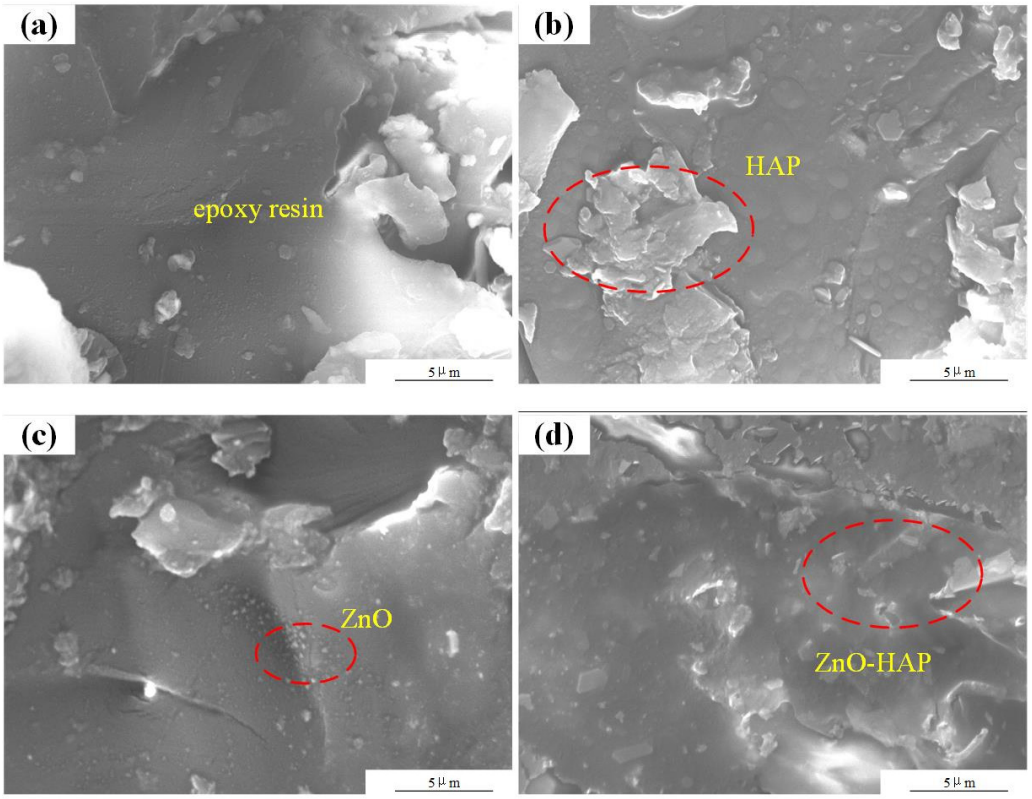

Figure 7. SEM morphologies of cross-section coatings: (**a**) pure epoxy resin, (**b**) HAP coating, (**c**) ZnO coating, and (**d**) ZnO-HAP (65 wt.% ZnO + 35 wt.% HAP)/epoxy resin coating.

To study the dispersion of ZnO-HAP nanocomposites in coatings, EDS was used to analyze the ZnO-HAP/epoxy resin. The element distribution is shown in Figure 8, and the surface elemental composition of ZnO-HAP nanocomposites is analyzed. The EDS patterns of the three selected spots are exhibited in Figure 9, and the EDS semi-quantitative results are listed in Table 2. Ca, P, and Zn elements were evenly distributed in the scanning surface of the coating, which proves that ZnO-HAP nanocomposites have good dispersion in an epoxy resin coating.

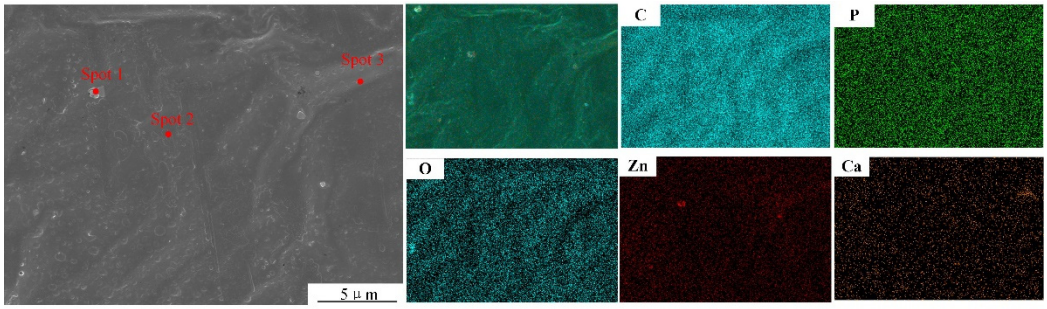

Figure 8. Secondary electron image and element distribution of ZnO-HAP (65 wt.% ZnO + 35 wt.% HAP)/epoxy coating.

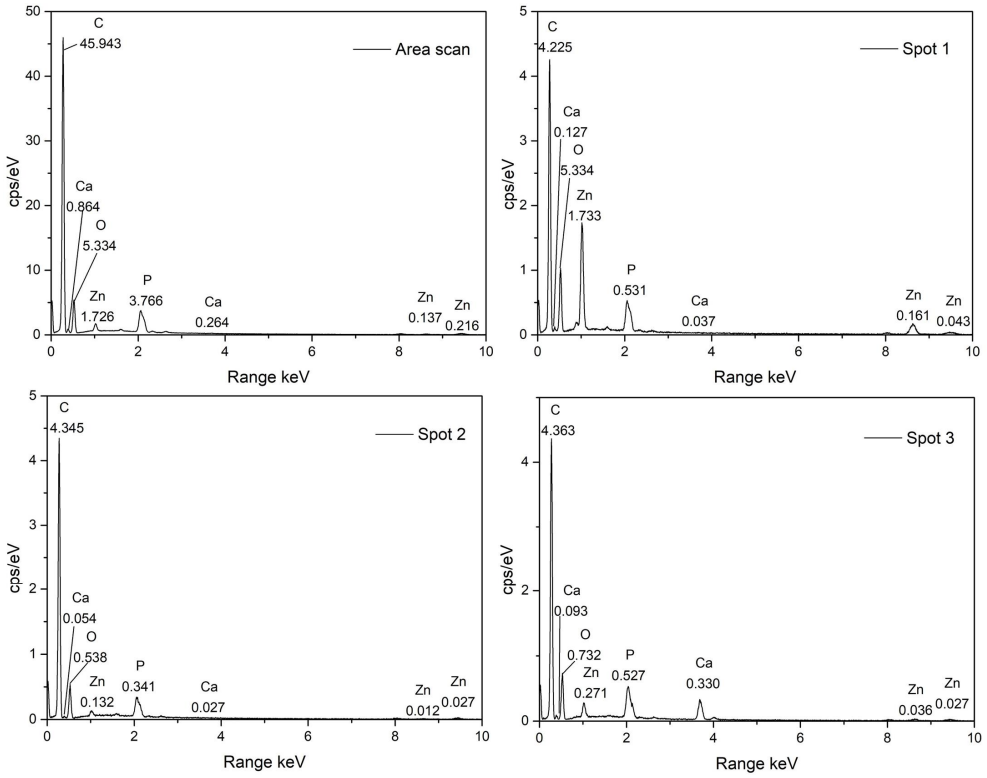

Figure 9. EDS analysis of area scan and three selected spots in Figure 7.

Table 2. EDS analysis results of the area scan and three selected spots shown in Figure 9.

Spot (wt.%)	C	O	Zn	P	Ca	Composition
Total area	75.47	21.52	2.48	0.45	0.08	ZnO, HAP, and epoxy resin
1	62.97	18.33	18.29	0.37	0.05	
2	75.83	21.91	0.34	0.02	1.90	
3	67.00	21.64	2.62	5.34	3.40	

3.3. Mechanical Property Analysis

To study the mechanical performance of different coatings, the hardness and adhesion of the coatings were investigated according to the GB/T6739-2006 pencil method to determine the hardness of paint film and the GB/T9286-1998 color paint and paint film grid test, respectively. The grade description of the adhesion test is shown in Table 3, where the higher the proportion of unshed lattice is, the higher the adhesion level of the coating. Table 4 shows the mechanical performance test results of different coatings. The hardness test results showed that the coating hardness of the ZnO-HAP composite pigment with 80 wt.% ZnO content was the lowest. From the adhesion test, the adhesion between the ZnO/epoxy resin and metal was the worst. With the proportion of HAP in pigment gradually increasing, the adhesion of the coating also steadily increased.

Table 3. Grades of GB/T9286-1998 color paint and paint film grid test.

Ratio (%)	100	95–100	85–95	65–85	35–65	0–36
Grade	0	1	2	3	4	5

Table 4. Results of mechanical performance of coatings with different components.

Coating	Pure Epoxy	HAP	ZnO	80 wt.% ZnO + 20 wt.% HAP	65 wt.% ZnO + 35 wt.% HAP	50 wt.% ZnO + 50 wt.% HAP
Hardness/H	4	6	4	2	4	6
Adhesion force/grade	0	0	2	1	0	0

3.4. Hydrophobic and Anti-Corrosion Property of Pigments

3.4.1. Measurement of the Contact Angle

An optical drop shape analyzer was used to measure the surface wettability of the coating, and the test results are shown in Table 5. The initial WCA value of the pure epoxy resin coating was 68.56°, which increased to 71.49° after adding nano-ZnO. The WCA value of the HAP/epoxy coating was only 35.91°, due to the presence of -OH on the HAP surface. -OH are hydrophilic groups, leading to poor epoxy coating hydrophobicity. The WCA value of ZnO-HAP composite coatings decreased with the increase of the HAP ratio.

Table 5. Results of water contact angle of coatings with different components.

Coating	Pure Epoxy	HAP	ZnO	80 wt.% ZnO + 20 wt.% HAP	65 wt.% ZnO + 35 wt.% HAP	50 wt.% ZnO + 50 wt.% HAP
WCA/degree	68.56	35.91	71.49	68.43	64.17	50.12

3.4.2. EIS Experiments

Figure 10 depicts the Nyquist plots of the mild steels coated with different coatings soaked in 3.5 wt.% NaCl solution for 24 and 72 h. In Nyquist plots, the resistance of the coating increased with the radius of the arc [18]. As shown in Figure 10, the arcs of the pure epoxy resin coating, HAP/epoxy resin, and ZnO/epoxy resin were small, indicating that the corrosion resistance of these three coatings is not excellent and mild steel electrodes are prone to damage in 3.5 wt.% NaCl solution. The Nyquist plots' ZnO-HAP/epoxy system arc after soaking for 24 and 72 h was always higher than the others. The steels coated with ZnO-HAP nanocomposites always exhibited more excellent corrosion resistance. These results indicate that adding the ZnO-HAP composite anti-corrosive pigment can significantly improve the anti-corrosive effect of the epoxy resin coating. Among the three kinds of ZnO-HAP coatings with different proportions, the ZnO-HAP coating with the ratio of 65 wt.% ZnO + 35 wt.% HAP had the best anti-corrosion performance. When the HAP content was too high (50 wt.% ZnO + 50 wt.% HAP), due to the influence of the hydrophilic group -OH on the HAP surface, the hydrophobicity of the coating surface decreased, and the anti-corrosion performance of the coating also decreased.

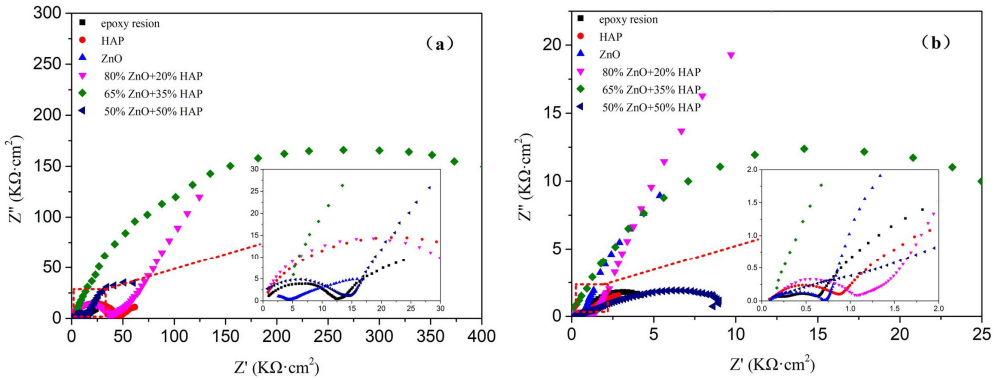

Figure 10. Nyquist plots of different coated steel samples soaked for different times: (**a**) soaked for 24 and (**b**) 72 h.

To further explore the anti-corrosive performance of the anti-corrosive pigment, the Bode plots of the coatings were analyzed. Figures 11 and 12 are Bode plots of different coatings soaked for 24 and 72 h, respectively, where (a) is the impedance modulus of each coating at different frequencies, and (b) is the phase angle plots of each coating at different frequencies. As shown in Figure 11, the coatings were still in the initial stage after soaking for 24 h. As can be seen from the plots, these phase angle curves have only one time constant, indicating that the organic coatings at this time are equivalent to an isolation layer with a significant resistance value and a small capacitance. At the initial immersion stage, as the electrolyte solution penetrated the organic coating, the impedance value in the curve gradually decreased with the increase of the horizontal coordinate. The electrolyte solution gradually penetrated the coatings, increasing the capacitance and decreasing the resistance.

As shown in Figure 12, the Bode plots after soaking for 72 h presented two characteristics of time constants. The one at higher frequency implies the penetration of electrolytes through the coating, and the other at middle frequency relates to the corrosion reaction. A region with a low slope can be observed from the middle frequency band in Figure 12a, which presents Warburg impedance characteristics. Due to the blocking effect of the additive particles in the organic coating, the electrolyte solution occupies the space between the particles and sinuous infiltration, and the mass transfer direction of the reaction particle is not parallel to the direction of the concentration gradient, which is called "tangential diffusion" [19]. From the impedance spectra in Figures 11 and 12, it can be seen that the resistance of the coating of 65 wt.% ZnO and 35 wt.% HAP anti-corrosive pigments was the largest, indicating the best anti-corrosive performance.

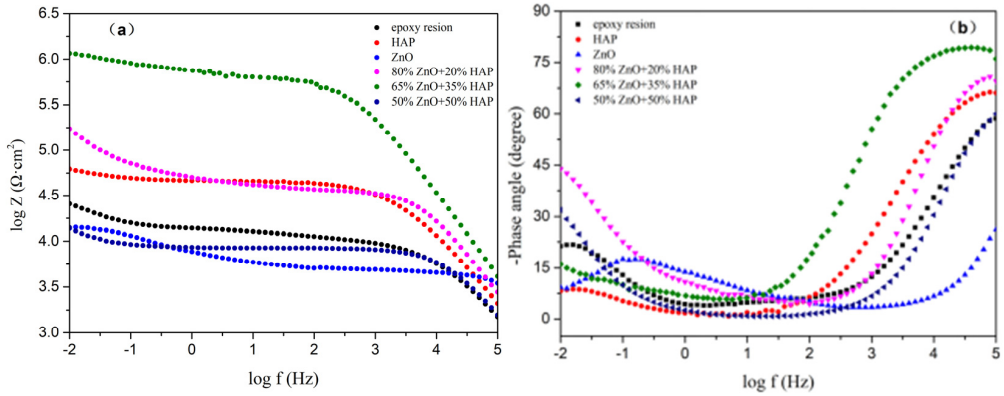

Figure 11. Bode plots of different electrodes soaked for 24 h: (**a**) impedance modulus spectrum and (**b**) phase angle spectrum.

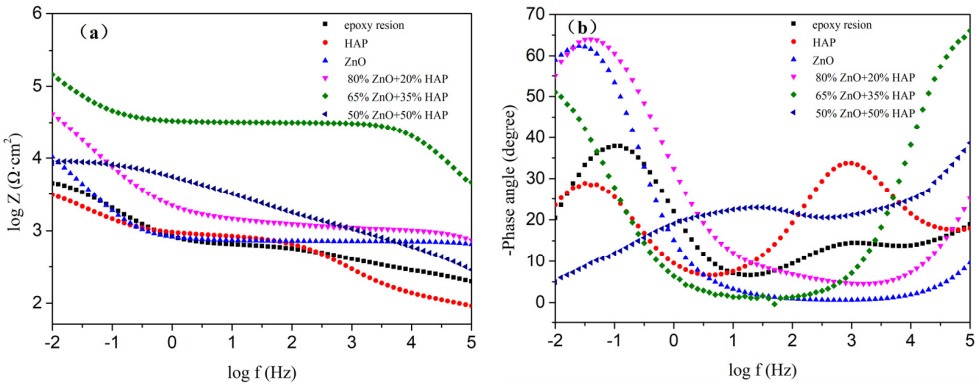

Figure 12. Bode diagrams of different electrodes soaked for 72 h: (**a**) impedance modulus spectrum and (**b**) phase angle spectrum.

The EIS results were fitted using the equivalent circuit shown in Figure 13. Figure 13a–c show the equivalent circuits of different coatings soaked for 24 and 72 h. In the circuit model, resistors R1, R2, and R3 correspond to solution resistance, coating resistance, and corrosion reaction linear polarization resistance, respectively [20,21]. Equivalent element CPE represents non-ideal capacitance, where CPE1 represents coating capacitance and CPE2 represents electric double-layer capacitance. The W element represents the Warburg component [22].

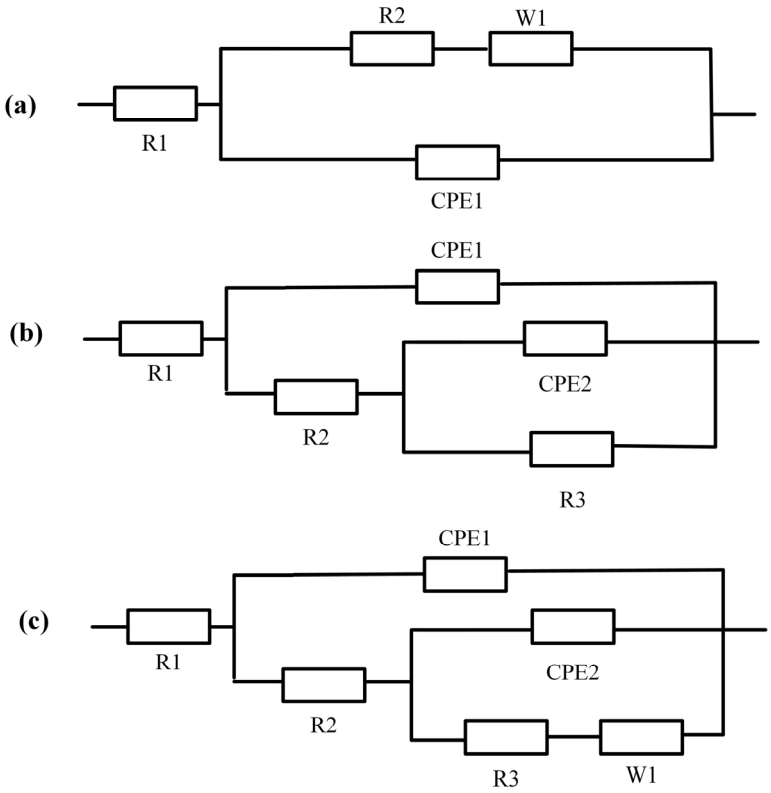

Figure 13. Equivalent circuit of steel electrodes with different coatings. (**a**) HAP (24 h) and ZnO-HAP (24 h), (**b**) pure epoxy resin (24 and 72 h), (**c**) HAP (72 h), ZnO (72 h) and ZnO-HAP (72 h).

As shown in Figure 13a, ZnO-HAP/epoxy coatings and HAP/epoxy coatings have sound anti-corrosion effects. The electrolyte did not penetrate the coating/base material interface after immersion for 24 h [23]. At this point, the coating is equivalent to an insulating layer with a considerable resistance value and a small capacitance value. Figure 13b shows the equivalent circuit of the pure epoxy resin coating. After soaking the pure epoxy resin

coating for 24 and 72 h, respectively, the electrolyte solution entering the coating reached saturation, and the electrolyte solution reached the coating/metal interface, resulting in corrosion and damage to the metal surface. Since no anti-corrosive pigment was added to the pure epoxy resin coating, the diffusion process of the electrolyte solution was not affected by the mass transfer process. Equivalent circuits of ZnO/epoxy coatings soaked for 24 and 72 h, HAP/epoxy coatings soaked for 72 h, and ZnO-HAP/epoxy coatings soaked for 72 h are shown in Figure 13c. Since the charge and discharge process of coating and the corrosion reaction of metal are affected by the mass transfer process, the Warburg element was added to the equivalent circuit.

The fitting parameters of the circuit are shown in Table 6. The resistance (R2) of ZnO-HAP/epoxy resin was significantly higher than that of the pure epoxy resin system, ZnO/epoxy system, and HAP/epoxy system. Significant resistance indicates that corrosive substances are difficult to enter the coating to corrode the mild steel. The high W value of ZnO-HAP/epoxy resin indicates that the ZnO-HAP nanocomposite can inhibit the diffusion of corrosive substances and thus slow down the corrosion reaction.

Table 6. EIS parameters of different coated electrodes soaked for 24 and 72 h, respectively.

Parameter	Blank/ 24 h	Blank/ 72 h	HAP 24 h	HAP 72 h	ZnO 24 h	ZnO 72 h	65 wt.% ZnO 35 wt.% HAP 24 h	65 wt.% ZnO 35 wt.% HAP 72 h
R1/ohm cm^2	49.11	83.26	117.20	81.39	38.07	139.80	807.50	321.40
R2/ohm cm^2	12,576.00	688.90	43,536.00	830.40	3956.00	642.80	375,580.00	31,432.00
Y1/ohm^{-1} cm^{-2} s^{-n}	6.37×10^{-8}	8.09×10^{-5}	1.27×10^{-8}	1.19×10^{-5}	4.48×10^{-8}	1.01×10^{-5}	7.64×10^{-9}	2.31×10^{-9}
n_1	0.67	0.33	0.78	0.65	0.63	0.33	0.72	0.86
Y2/ohm^{-1} cm^{-2} s^{-n}	0.00031	0.00074	-	0.0016	0.00014	0.00095	-	6.03×10^{-5}
n_2	0.59	0.80	-	0.65	0.33	0.86	-	0.75
W/ohm cm^2	-	-	66,015	7060.26	6842.00	10,760.00	1.30×10^6	425,480.00
Y_w/ohm^{-1} cm^{-2} s^{-n}	-	-	398.30	418.30	10,251.00	42.57	220.30	92.42
n_w	-	-	0.39	0.11	0.28	0.37	0.18	0.47
R3	51,762.00	5668.0	-	475.40	59,470.00	39,401.00	-	1.17×10^6

Note: "-" means there is no such data in the circuit fitting result.

The deviation from pure capacity reflected by CPE indicates the roughness and energy dissipation of the electrode surface [24,25]. The following formula expresses the impedance of a CPE element:

$$Z_{CPE} = \frac{1}{Y_0(jw)^n} \quad (4)$$

where ω is the angular frequency (rad/s), and n is the power number, defined as $n = \alpha (\pi/2)$ (α is the constant phase angle of CPE (rad)), which indicates the deviation of the interface from the ideal capacitor, representing resistive, Warburg, and capacitive behaviors for $n = 0$, 0.5, and 1, respectively [26,27]. Y_0 (admittance) is a CPE constant ($s^n \cdot \Omega^{-1} \cdot Cm^{-2}$), directly proportional to the active surface area exposed to the electrolyte. Both Y_0 and n are independent of frequency [28,29].

The parameter values estimated by impedance spectrum fitting analysis are summarized in Table 5. As described in Table 6, the polarization resistance corresponding to R2 is the highest, indicating that the epoxy coating has better corrosion resistance due to ZnO-HAP. Y_1 is related to the active surface area involved in electrochemical reactions. With the addition of anti-corrosive pigments to the coating, this value decreased (Y_1 value was highest for pure epoxy coating), which can be attributed to the role of anti-corrosive pigments as a barrier during corrosion, which reduces the porosity of the epoxy coating and makes it more difficult for the metal surface to contact the electrolyte [30,31]. An increase in n_1 means a decrease in the inhomogeneity and roughness of the coating surface, indicating a reduction in the corrosion sensitivity of the coating relative to the substrate. A higher n value means a better surface performance of the coatings [32]. In Table 6, the n_1 values of HAP/epoxy coatings were the largest, followed by ZnO-HAP (65% ZnO, 35% HAP) coatings, and the ZnO/epoxy coating had the smallest n_1 value. The results show that the ZnO-HAP/epoxy system has better surface performance. With the extension of the immersion time, the Y_1 value of the ZnO-HAP/epoxy coating decreased, and the n_1 value

increased due to the increased density of the coating due to the refractory chlorine apatite solidified by HAP after the chloride ion entered the coating.

3.4.3. Polarization Curve Measurements

The corrosion rates of different mild steels were investigated by potentiodynamic polarization curves (Figure 14). Polarization curves are composed of anode and cathode polarization curves: Tafel anode slope (b_a) and Tafel cathode slope (b_c) can be fitted, respectively, and corrosion potential (E_{corr}) and corrosion current density (I_{corr}) can also be obtained by the Tafel extrapolation method [33]. These Tafel parameters can estimate the anti-corrosion performance of anti-corrosive pigments. The E_{corr} value is proportional to the corrosion resistance of the coating, and the I_{corr} value is proportional to the corrosion inhibition performance of the coating. The fitting parameters are shown in Table 7.

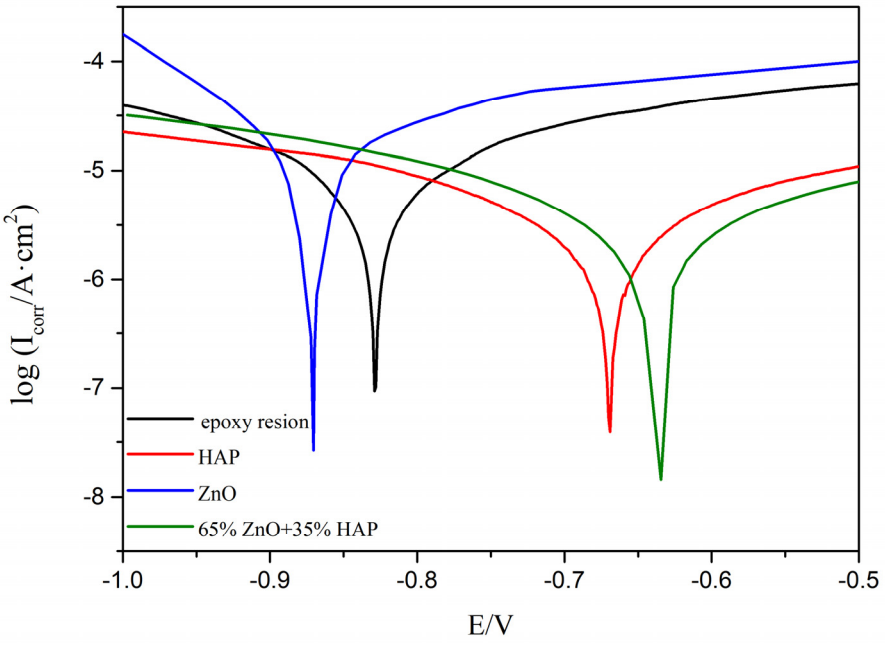

Figure 14. Tafel curves of different mild steel electrodes.

Table 7. Dynamic polarization curve parameters of different mild steel electrodes.

Samples	E_{corr} (V)	I_{corr} (μA cm^{-2})	b_a (V/dec)	b_c (V/dec)	R_p (Ohm·cm^{-2})
Pure epoxy	−0.828	34.410	6.587	1.906	4663
HAP	−0.666	13.170	3.461	3.679	14,700
ZnO	−0.869	71.923	2.381	1.052	2446
65% ZnO + 35% HAP	−0.640	2.338	0.984	0.548	163,400

From Table 7, the E_{corr} value of pure epoxy resin was −0.828 V and the I_{corr} value was 34.410 μA/cm^2, while the E_{corr} value of ZnO/epoxy resin was −0.869 V and the I_{corr} value was 71.923 μA/cm^2. The reason for this result is that the adhesion between the ZnO/epoxy resin and metal was the worst: the high polarization destabilizes this type of coating, and it peels off the substrate and cracks, and this creates accessibility for the flow of the corrosive medium to the steel. Thus, it shows a slightly worse result than pure epoxy. The E_{corr} value of ZnO-HAP/epoxy was the highest when the ZnO to HAP ratio was 65:35 wt.% and its I_{corr} value was only 1.2 μA/cm^2. High E_{corr} and low I_{corr} values confirmed that ZnO-HAP nanocomposites could effectively inhibit the corrosion reaction. The results show that ZnO and HAP can protect mild steel.

3.4.4. Anti-Corrosion Mechanism

Figure 15 illustrates the anti-corrosion mechanism of the ZnO-HAP nanocomposites. As shown in Figure 15a, for the coating of pure epoxy resin with no anti-corrosion pigment, electrolyte solution can penetrate directly through the coating to the steel substrate. Cl^- in the electrolyte easily causes local corrosion, such as pitting corrosion and gap corrosion, and destroys metal passivation. As shown in Figure 15b, ZnO adheres to the surface of the HAP sheets to form a complex staggered structure, filling the pores of the epoxy resin and complicating the permeating path of the aggressive species. Meanwhile, the substitution reaction between Cl^- in solution and -OH on HAP produced stable chlorapatite [34], which improved the corrosion resistance of the coating. Therefore, the synergistic anti-corrosion effect of ZnO and HAP can provide adequate protection for mild steel.

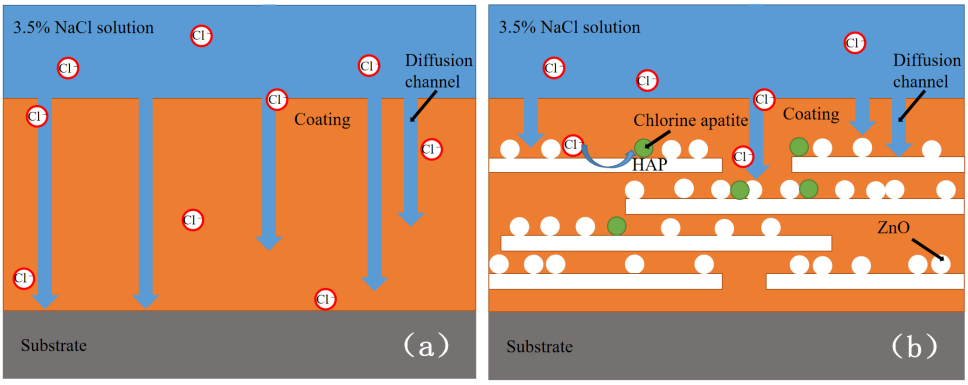

Figure 15. Anti-corrosion mechanism diagram of coatings: (**a**) epoxy resin and (**b**) 65 wt.% ZnO + 35 wt.% HAP.

4. Conclusions

The ZnO-HAP nanocomposite anti-corrosive pigment was successfully prepared using the hydrothermal in situ synthesis technique, loading ZnO onto the HAP sheets. Electrochemical analysis showed that the anti-corrosive effect was the best when the ratio of ZnO and HAP in the ZnO-HAP anti-corrosive pigment was 65:35 wt.%. By combining zinc oxide with HAP, the adverse effect of zinc oxide on the mechanical properties (adhesion) of the epoxy resin coating was effectively improved, and the adhesion of the coating improved from grade 2 to grade 0. Similarly, zinc oxide was attached to the HAP surface, which improved the hydrophobicity of HAP. The complementary mechanism of zinc oxide and HAP significantly improved the coating's anti-corrosion effect, reduced the porosity of the epoxy coating, and complicated corroded materials' penetration path. At the same time, Cl^- penetrated the coating and exchanged with hydroxyl groups in the HAP crystal to form insoluble chlorine apatite, which was fixed in the coating to further decrease the pores of the coating and increase the service life.

Author Contributions: Writing—review and editing, resources, methodology, X.X.; writing—review and editing, methodology, investigation, formal analysis, H.W.; resources, project administration, funding acquisition, conceptualization, J.W.; formal analysis, data curation, Z.C.; investigation, X.Z.; formal analysis, M.L. All authors have read and agreed to the published version of the manuscript.

Funding: There is no funding for our project.

Institutional Review Board Statement: Not applicable.

Informed Consent Statement: Not applicable.

Data Availability Statement: Not applicable.

Conflicts of Interest: The authors declare no conflict of interest.

References

1. Chilkoor, G.; Karanam, S.P.; Star, S.; Shrestha, N.; Sani, R.K.; Upadhyayula, V.K.; Ghoshal, D.; Koratkar, N.A.; Meyyappan, M.; Gadhamshetty, V. Hexagonal boron nitride: The thinnest insulating barrier to microbial corrosion. *ACS Nano* **2018**, *12*, 2242–2252. [CrossRef] [PubMed]
2. Guo, Q.; Chen, H. Development prospect of heavy-duty anti-corrosive coatings. *Chem. Prog.* **2003**. Available online: https://dysw.cnki.net/kcms/detail/detail.aspx?filename=ZGTU2003S1001&dbcode=CJFQ&dbname=CJFD2003&v= (accessed on 10 March 2022).
3. Bian, J.; Wang, W.; Guan, C. Research progress of organic coatings for metal corrosion protection. *J. Mater. Sci. Eng.* **2003**, *21*, 769–772.
4. Zaarei, D.; Sarabi, A.A.; Sharif, F.; Kassiriha, S.M. Structure, properties and corrosion resistivity of polymeric nanocomposite coatings based on layered silicates. *J. Coat. Technol. Res.* **2008**, *5*, 241–249. [CrossRef]
5. Zheng, J.; Ozisik, R.; Siegel, R.W. Disruption of self-assembly and altered mechanical behavior in polyurethane/zinc oxide nanocomposites. *Polymer* **2005**, *46*, 10873–10882. [CrossRef]
6. El Saeed, A.M.; El-Fattah, M.A.; Azzam, A.M. Synthesis of ZnO nanoparticles and studying its influence on the antimicrobial, anti-corrosion, and mechanical behavior of polyurethane composite for surface coating. *Dyes Pigment.* **2015**, *121*, 282–289. [CrossRef]
7. Le, H.L.T.; Lazzari, R.; Goniakowski, J.; Cavallotti, R.; Chenot, S.; Noguera, C.; Jupille, J.; Koltsov, A.; Mataigne, J.M. Tuning Adhesion at Metal/Oxide Interfaces by Surface Hydroxylation. *J. Phys. Chem. C* **2017**, *21*, 11464–11471. [CrossRef]
8. Xue, X.Z.; Zhang, J.Y.; Zhou, D.; Liu, J.K. In-situ bonding technology and excellent anti-corrosion activity of graphene oxide/hydroxyapatite nanocomposite pigment-ScienceDirect. *Dyes Pigment.* **2019**, *160*, 109–118. [CrossRef]
9. Wei, D.; Qi, X.; Li, D. Research status of inorganic modification of organic anti-corrosive coatings. *Sci. Wealth* **2011**, 17–18.
10. Hu, X.J.; Liu, J.K.; Qin, X.Y.; Huang, J.; Yi, Y. Facile synthesis of hydroxylapatite nanostructures with various morphologies. *Nano* **2009**, *4*, 165–170. [CrossRef]
11. Fihri, A.; Len, C.; Varma, R.S.; Solhy, A. Hydroxyapatite: A review of syntheses, structure, and applications in heterogeneous catalysis. *Coord. Chem. Rev.* **2017**, *347*, 48–76. [CrossRef]
12. Wang, J.; Shaw, L.L. Morphology-enhanced low-temperature sintering of nanocrystalline hydroxyapatite. *Adv. Mater.* **2007**, *19*, 2364–2369. [CrossRef]
13. Gao, F.; Wang, Q.; Gao, N.; Yang, Y.; Cai, F.; Yamane, M.; Gao, F.; Tanaka, H. Hydroxyapatite/chemically reduced graphene oxide composite: Environment-friendly synthesis and high-performance electrochemical sensing for hydrazine. *Biosens. Bioelectron.* **2017**, *97*, 238–245. [CrossRef] [PubMed]
14. Harja, M.; Ciobanu, G. Studies on adsorption of oxytetracycline from aqueous solutions onto hydroxyapatite. *Sci. Total Environ.* **2018**, *628–629*, 36–43. [CrossRef] [PubMed]
15. Xue, X.Z.; Tang, S.; Yuan, X.Y.; Yue, Y.B.; Liu, J.K.; Yang, X.H. One-step crushing & cladding technology and enhanced anti-corrosion activity of $Zn_3(PO_4)_2$@$AlH_2P_3O_{10}$ pigment. *J. Alloy. Compd.* **2018**, *744*, 837–848.
16. Stango SA, X.; Karthick, D.; Swaroop, S.; Mudali, U.K.; Vijayalakshmi, U. Development of hydroxyapatite coatings on laser textured 316 LSS and Ti-6Al-4V and its electrochemical behavior in SBF solution for orthopedic applications. *Ceram. Int.* **2018**, *44*, 3149–3160. [CrossRef]
17. González, M.G.; Cabanelas, J.C.; Baselga, J. *Applications of FT-IR on Epoxy Resins-Identification, Monitoring the Curing Process, Phase Separation and Water Uptake*; InTech: London, UK, 2012; pp. 261–284.
18. Samad, U.A.; Alam, M.A.; Anis, A.; Abdo, H.S.; Shaikh, H.; Al-Zahrani, S.M. Nanomechanical and Electrochemical Properties of ZnO-Nanoparticle-Filled Epoxy Coatings. *Coatings* **2022**, *12*, 282. [CrossRef]
19. Cao, C.; Zhang, J. *Introduction to Electrochemical Impedance Spectroscopy*; Science Press: Beijing, China, 2002; pp. 118–185.
20. Ramezanzadeh, B.; Ghasemi, E.; Askari, F.; Mahdavian, M. Synthesis and characterization of a new generation of inhibitive pigment based on zinc acetate/benzotriazole: Solution-phase and coating phase studies. *Dyes Pigment.* **2015**, *122*, 331–345. [CrossRef]
21. Ates, M.; Uludag, N. Synthesis of 6-(3,6-di(thiophene-2-yl)-9H-carbazole-9-yl)- hexanoic acid, alternating copolymer formation, characterization and impedance evaluations. *Polym.-Plast. Technol. Eng.* **2012**, *51*, 640–646. [CrossRef]
22. Ates, M.; Osken, I.; Ozturk, T. Poly(3,5-dithiophene-2-yldithieno[3,2-b;2′,3′d] thiophene-co-ethylene dioxythiophene)/glassy carbon electrode formation and electrochemical impedance spectroscopic study. *J. Electrochem. Soc.* **2012**, *159*, E115–E121. [CrossRef]
23. Yingnan, W.; Xueyan, D.; Tianlu, X.; Lijie, Q.; Chunling, Z. Preparation and Anti-corrosion properties of silane grafted nano-silica/epoxy composite coating. *J. Chem. Coll. Univ.* **2018**, *39*, 1843–1845.
24. Liu, C.; Du, P.; Zhao, H.; Wang, L. Synthesis of l-histidine-attached graphene nanomaterials and their application for steel protection. *ACS Appl. Nano Mater.* **2018**, *1*, 1385–1395. [CrossRef]
25. Yabuki, A.; Shiraiwa, T.; Fathona, I.W. pH-controlled self-healing polymer coatings with cellulose nanofibers providing an effective release of corrosion inhibitor. *Corros. Sci.* **2016**, *103*, 117–123. [CrossRef]
26. Bu, Y.; Chen, Z. Highly efficient photoelectrochemical anti-corrosion performance of C_3N_4@ZnO composite with quasi-shell-core structure on 304 stainless steel. *RSC Adv.* **2014**, *4*, 45397–45406. [CrossRef]

27. Deyá, M.; Sarli, A.R.D.; Amo, B.D.; Romagnoli, R. Performance of anti-corrosive coatings containing tripolyphosphates in aggressive environments. *Ind. Eng. Chem. Res.* **2008**, *47*, 7038–7047. [CrossRef]
28. Ramezani-Varzaneh, H.A.; Allahkaram, S.R.; Isakhani-Zakaria, M. Effects of phosphorus content on corrosion behavior of trivalent chromium coatings in 3.5 wt% NaCl solution. *Surf. Coat. Technol.* **2014**, *244*, 158–165. [CrossRef]
29. Jorcin, J.B.; Orazem, M.E.; Pébère, N.; Tribollet, B. CPE analysis by local electrochemical impedance spectroscopy. *Electrochim. Acta* **2006**, *51*, 1473–1479. [CrossRef]
30. Frangini, S.; Loreti, S. The role of temperature on the corrosion and passivation of type 310S stainless steel in eutectic (Li+K) carbonate melt. *J. Power Sources* **2006**, *160*, 800–804. [CrossRef]
31. Cho, K.W.; Rao, V.S.; Kwon, H.S. Microstructure and electrochemical characterization of trivalent chromium based conversion coating on zinc. *Electrochim. Acta* **2007**, *52*, 4449–4456. [CrossRef]
32. Isakhani-Zakaria, M.; Allahkaram, S.R.; Ramezani-Varzaneh, H.A. Evaluation of corrosion behaviour of Pb-Co_3O_4 electrodeposited coating using EIS method. *Corros. Sci.* **2019**, *157*, 472–480. [CrossRef]
33. Miao, M.; Yuan, X.Y.; Wang, X.G.; Lu, Y.; Liu, J.K. One step self-heating synthesis and their excellent anti-corrosion performance of zinc phosphate/benzotriazole composite pigments. *Dyes Pigment.* **2017**, *141*, 74–82. [CrossRef]
34. Bouyarmane, H.; Gouza, A.; Masse, S.; Saoiabi, S.; Saoiabi, A.; Coradin, T.; Laghzizil, A. Nanoscale conversion of chlorapatite into hydroxyapatite using ultrasound irradiation. *Colloids Surf. A Physicochem. Eng. Asp.* **2016**, *495*, 187–192. [CrossRef]